Bull. Mater. Sci., Vol. 38, No. 2, April 2015, pp. 557–563. © Indian Academy of Sciences.

Thermal and electrical properties of $60V_2O_5$–$5P_2O_5$–$(35-x)B_2O_3$–$xCeO_2$ ($1 \leq x \leq 5$) glasses

R V BARDE[1] and S A WAGHULEY[2,*]

[1]Department of Engineering Physics, H.V.P.M. College of Engineering & Technology, Amravati 444 605, India
[2]Department of Physics, Sant Gadge Baba Amravati University, Amravati 444 602, India

MS received 19 November 2013; revised 8 May 2014

Abstract. **The samples of composition $60V_2O_5$–$5P_2O_5$–$(35-x)B_2O_3$–$xCeO_2$, $x = 1$, 2, 3, 4 and 5 mol% were prepared by the melt-quench method. The prepared samples were characterized by X-ray diffraction, thermogravimetric-differential thermal analysis and impedance spectroscopy. The activation energies were evaluated using glass transition temperature (T_g) and peak temperature of crystallization (T_c). The dependence of activation energy on composition was discussed. AC conductivity of samples has been analysed. Electrical conductance and capacitance were measured over a frequency range of 20 Hz–1 MHz and a temperature range of 303–473 K. At room temperature, maximum value of electrical conductivity was observed to be 0.0024 S cm^{-1} for $x = 1$. The samples show semiconducting features predominantly based on an ionic mechanism.**

Keywords. **Glasses; electrical and thermal properties; impedance spectroscopy.**

1. Introduction

Electrically conducting glasses have been attracted much attention in the field of materials science and solid-state chemistry. Vanadium pentoxide is known to have a structure composed of VO_5 pyramids. The vanadates-based glasses show semiconducting behaviour due to electron hopping between V^{4+} and V^{5+} ions.[1–4] Structural probing of semiconducting transition metal oxide extend applications of such glasses for memory and switching devices. Although various vanadium ions-doped glasses have been investigated, most of them are restricted to structural studies. Hence, there is a scope to investigate the influence of vanadium ions alkaline earth borate glasses, through impedance study.[5,6] There are several questions about the frequency dependence of electrical properties of metal oxide glasses and the complex quantities such as AC conductivity and permittivity. This difficulty can be overcome by measuring AC electrical response over a wide range of frequencies.[1–4] The rare earth and transition metal containing glasses have been widely studied using structural and optical spectroscopy due to their several applications. Some of the possible applications are optical amplifiers in telecommunication,[7] phosphorescence materials and electrochemical batteries.[8] Rare earth metal ions when added to borate act as network modifiers and change the properties of glasses. In rare earth metals, cerium oxide-doped glasses have been studied by many researchers because of their applications as biosensor,[9] solid oxide fuel cells,[10] corrosion protection,[11] photoluminescent material[12] and also used in tunable solid-state lasers operating in the UV, violet and blue regions.[13] Cerium-based scintillates are used for gamma ray detection.[14] The idea of ionic conduction in cerium lithium glasses has given by Mansour.[15] Barde and Waghuley[1–4] have also studied the DC electrical behaviour of CeO_2-doped glasses.

Inspiring from the above discussion, we prepared glass system $60V_2O_5$–$5P_2O_5$–$(35-x)B_2O_3$–$xCeO_2$, $x = 1$, 2, 3, 4 and 5 mol% to analysed conductivity as a function of temperature along with dielectric and thermal properties. The thermal study was performed to ascertain the stability of glass. The conductivity was determined using impedance spectroscopy of these glasses at different temperature. The prepared samples were characterized by X-ray diffraction (XRD) and thermogravimetric-differential thermal analysis (TG-DTA).

2. Experimental

The glass systems of composition $60V_2O_5$–$5P_2O_5$–$(35-x)B_2O_3$–$xCeO_2$, $x = 1$, 2, 3, 4 and 5 mol%, were prepared by a conventional melt-quenching method. AR grade (SD Fine, India) chemicals were used in this investigation, which were weighed and mixed together. This mixture was homogenized and melted in silica crucible at 900°C for 3 h and the melt was stirred to remove CO_2. After melting, the mixture was poured out onto a nonmagnetic stainless-steel substrate maintained at temperature 15°C and pressed with another stainless-steel substrate. In this way, quenching was achieved by rapid cooling of molten mixture to substrate temperature. To avoid internal strains, the samples were annealed at 200°C for 1 h and then cooled slowly to room temperature.

*Author for correspondence (sandeepwaghuley@sgbau.ac.in)

XRD analysis of the samples was carried out using CuKα radiation (1.54 Å) by RIGAKU X-ray diffractometer in the 2θ range of 10–70°. TG-DTA was carried out on Shimadzu DTG-60h thermal analyser under nitrogen flow at the heating rate of 10°C min^{-1}. The temperature of samples varied from room temperature to 600°C.

For electrical measurements, samples were polished and conducting silver paste was deposited on both sides. The sample area was taken to be the area exposed to the electrode surface. The temperature dependence of electrical conductivity σ and dielectric constant ε' were measured using LCR meter, Agilent Technology, Singapore. The measurements were performed in a frequency region of 20 Hz–1 MHz and a temperature range of 303–473 K.

3. Results and discussion

3.1 *XRD analysis*

Figure 1 depicts the XRD patterns of the $60V_2O_5$–$5P_2O_5$–$(35-x)B_2O_3$–$xCeO_2$, $x = 1$, 2, 3, 4 and 5 mol%, a broad diffused peak and the absence of well-defined peaks clearly pointed out the formation of glass. There was no characteristic peak, which corresponds to any crystalline phase and therefore it can be inferred that the obtained samples are amorphous. The amorphous hallow appears at the same 2θ-position.

3.2 *Thermal analysis*

The study regarding phase transition and thermal stability during heat treatment to the sample were analysed through the TG-DTA technique carried out from room temperature to 600°C in nitrogen atmosphere. TGA curves displayed in figure 2a and b clearly shows the thermal dehydration in glasses. Thermograms indicate 13% weight loss within the temperature range of 30–200°C corresponding to the loss of water molecules, after which a gradual weight loss is observed till ∼300°C. This may be due to the condensation of structural hydroxyl groups. On the entire range of temperature, sample shows nearly 22% weight loss.

Figure 2a and b shows the DTA profiles of the glasses for 1 and 5 mol% of CeO_2. This kind of thermal behaviour has been reported for many glass systems.[1–4,16] On the basis of these observations, we identify an endothermic peak between 95 and 120°C as glass transition temperatures (T_g). Another sharp endothermic peak between 130 and 140°C followed by an exothermic peak may be related to some of the physical changes like melting or decomposition followed by amorphous to crystalline phase transition, which occurred in system around temperature range 130–140°C.[17] The T_g of the annealed glasses were 96 and 113°C for the sample $60V_2O_5$–$5P_2O_5$–$34B_2O_3$–$1CeO_2$ and $60V_2O_5$–$5P_2O_5$–$30B_2O_3$–$5CeO_2$ whereas, T_c of the annealed glasses were 130 and 137°C, respectively. The thermal stability

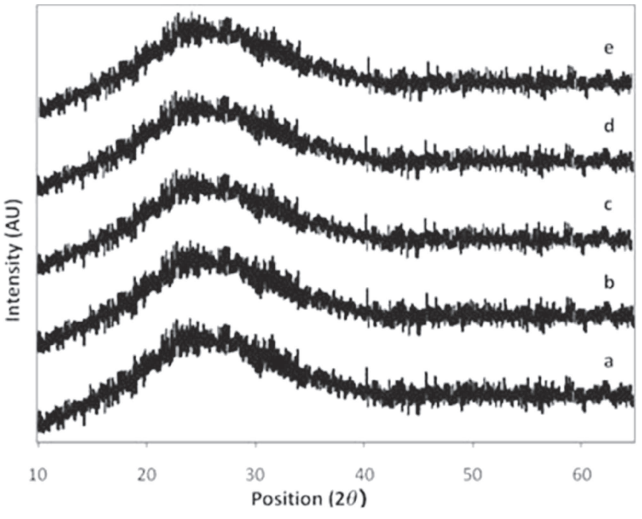

Figure 1. XRD of $60V_2O_5$–$5P_2O_5$–$(35-x)B_2O_3$–$xCeO_2$ for (**a**) $x = 1$ mol%, (**b**) $x = 2$ mol%, (**c**) $x = 3$ mol%, (**d**) $x = 4$ mol% and (**e**) $x = 5$ mol%.

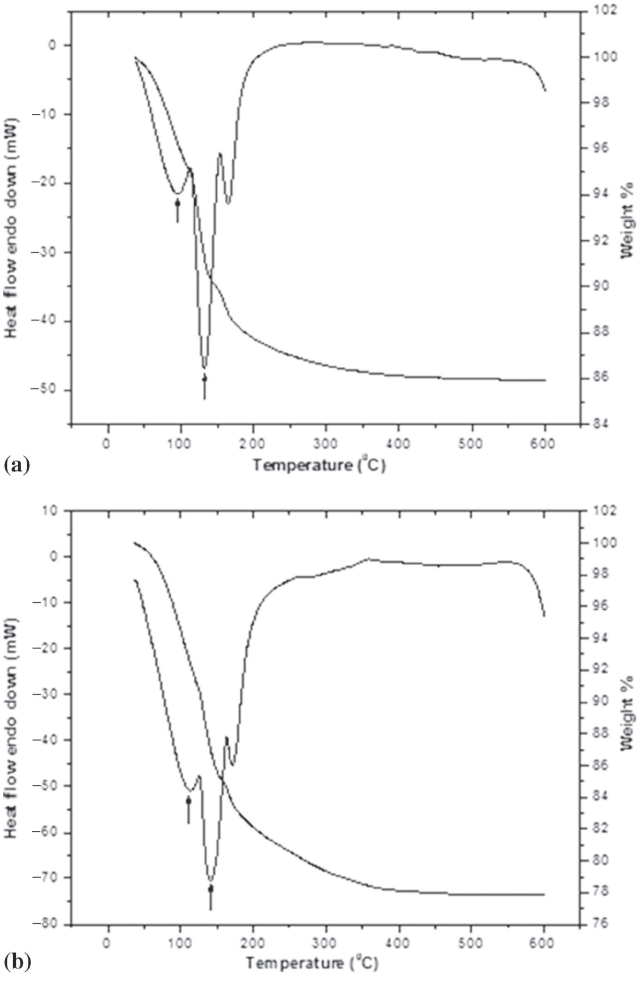

Figure 2. TG-DTA plot of (**a**) $60V_2O_5$–$5P_2O_5$–$34B_2O_3$–$1CeO_2$ and (**b**) $60V_2O_5$–$5P_2O_5$–$30B_2O_3$–$5CeO_2$.

$(T_c - T_g)$ decreases with the increase in the content of CeO_2. The thermal stability of the glass was found to be excellent for the composition with $x = 1$.

The DTA curve and its derivatives (DDTA) are simultaneously recorded as shown in figure 3a and b. Two inflections point that is maximum and minimum slopes of DTA peak corresponding to maximum and minimum of DDTA double peaks are obtained. Therefore, the temperature T_{f_1} and T_{f_2} for endothermic and exothermic peaks can be easily and exactly detected on DDTA curve. The activation energy (E_a) of first-order reaction using temperature of two inflection points T_{f_1} and T_{f_2} was derived from Equation (1). The endo- and exo-activation energies were found to be 14.25 and 243.89 kJ mol^{-1} (estimated from peaks at 349 and 366°C), for the sample $60V_2O_5$–$5P_2O_5$–$34B_2O_3$–$1CeO_2$ and 11.70 and 119.88 kJ mol^{-1} for the sample $60V_2O_5$–$5P_2O_5$–$30B_2O_3$–$5CeO_2$, respectively.[18]

$$\frac{E_a}{R}\left(\frac{1}{T_{f_1}} - \frac{1}{T_{f_2}}\right) = 1.92, \tag{1}$$

where R is the universal gas constant.

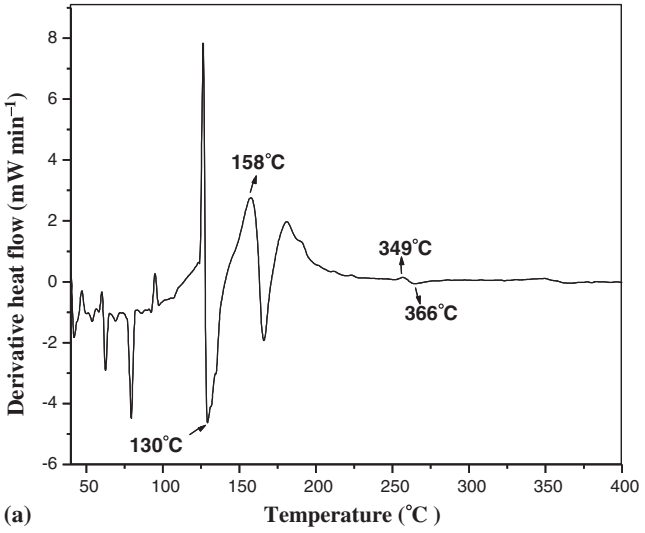

(a)

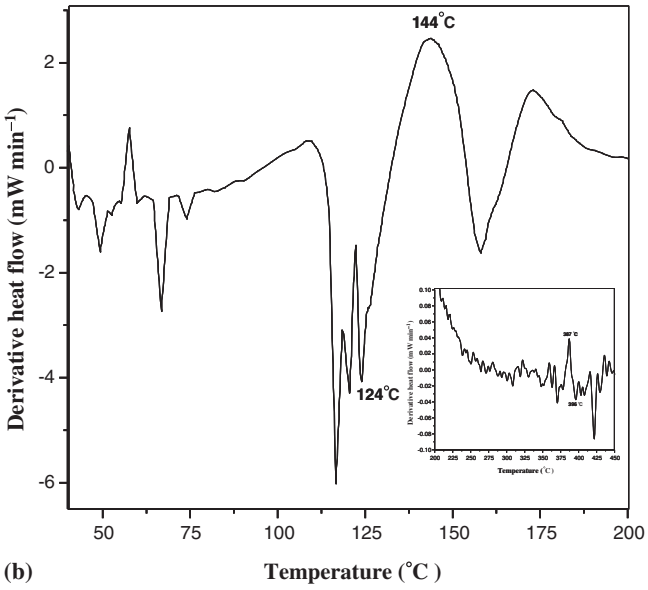

(b)

Figure 3. Simultaneous recorded DDTA curve of (**a**) $60V_2O_5$–$5P_2O_5$–$34B_2O_3$–$1CeO_2$ and (**b**) $60V_2O_5$–$5P_2O_5$–$30B_2O_3$–$5CeO_2$.

3.3 *Electrical conductivity measurements*

Complex impedance measurements were carried out to determine the electrical conductivity and AC behaviour of glasses over a range of temperature and frequencies. Figure 4 shows the impedance plot (Z' *vs.* Z'') for 2 mol% of CeO_2 at different temperatures. Such shapes are typically observed in superionic solids exhibiting lattice disorder.[19] The centre of semicircle was found below Z'-axis. This behaviour shows that relaxation nature of ions is non-Debye. As temperature increases, radius of semicircle decreases, which shows an activated conduction mechanism.[20–23] The impedance plot shows a low frequency spike and a small portion of the semicircle. The semicircle at high frequency and low frequency region is due to the bulk relaxation and interfacial effects, respectively. Semicircle was successfully fitted using parallel RC circuit. Figure 5 shows impedance plot for all samples at 393 K, exhibited same behaviour. From semicircle the associated values of capacitance (C) can be determined by using relation $2\pi f RC = 1$. Here R is the value of real part of impedance at the top of semicircle. The values of R and C of parallel RC circuit for different temperature are listed in table 1. From the peak maxima relaxation time of samples are calculated by using relation $\omega\tau = 1$. The typical plot of relaxation time against inverse of temperature is shows in figure 6 for the system $60V_2O_5$–$5P_2O_5$–$(35-x)B_2O_3$–$xCeO_2$ with $x = 2$ mol%. It is found that the relaxation time obeys Arrhenius relation

$$\tau = \tau_0 \exp\left(\frac{E_\tau}{KT}\right) \tag{2}$$

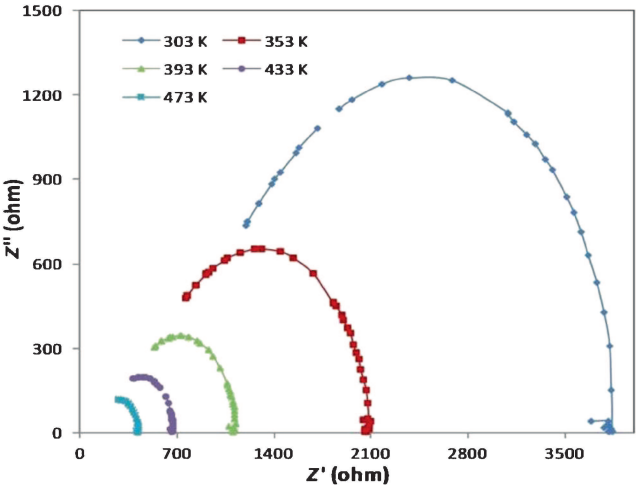

Figure 4. Cole–cole plot of $60V_2O_5$–$5P_2O_5$–$33B_2O_3$–$2CeO_2$.

where E_τ is the activation energy. From the activation energy, we can predict that the relaxation time is determined by the flow of charge carriers. It is cleared that conductivity is influenced by both frequency and temperature and AC conductivity may be due to increase in thermally activated drift mobility of ions according to polaron hopping conduction mechanism.[1–4,21,22,25,26]

DC resistance of the samples is obtained from intersection of semicircle with the real axis at low frequency. With increasing temperature, intercepts of semicircle shift towards the origin. DC conductivity (σ_{dc}) was calculated using sample dimensions. Its value increases with the increase in temperature that is with the increase in temperature, bulk resistance of the sample decreases and electrical conductivity thus shows a gradual enhancement, which is activated conduction mechanism. The reciprocal temperature dependence of the DC conductivity is shown in figure 7. The plot shows that DC conductivity exhibits an Arrhenius-type temperature dependence given by the relation

$$\sigma_{dc} = \sigma_0 \exp\left(-\frac{E_{dc}}{KT}\right). \quad (3)$$

The activation energy, E_{dc} was calculated from the least-square straight-line fitting of plot. The values of E_{dc} for different compositions at room temperature are given in table 1. It is observed that conductivity shows a random nature. It is maximum for 1 mol% of CeO_2 and decreases for 2 h mol% of CeO_2. If we further increase the mol% of CeO_2, conductivity increases up to 4 mol% and beyond this it decreases. The maximum in conductivity corresponds with minimum of activation energy. This could be explained on the basis of Mixed Glass Former effect.[24] The explanation for enhancement in conductivity is given on the basis of the Anderson and Stuart model. According to this model, as one of the glass former ion is substituted by another glass former ion, the average interionic bond distance changes. It becomes larger/smaller depending on substituting ion is larger/smaller. Thus with the addition of 1 mol% CeO_2, the structure becomes loose and hence conductivity increases.[27] The decrease in conductivity beyond 1 mol% CeO_2 is due to elimination of the number of non-bridging oxygens. The further enhancement in conductivity may be due to creation of NBOs.[28,29]

Figure 8 shows frequency-dependent conductivity plot of $\log(\omega)$ *vs.* $\log(\sigma)$ for the composition $60V_2O_5$–$5P_2O_5$–$(35-x)B_2O_3$–$1CeO_2$ at various temperatures. In low frequency region conductivity is found to be almost frequency-independent, suggesting that the ionic diffusion is random less via activated hopping process. At high frequency region, dispersion in conductivity has been observed.

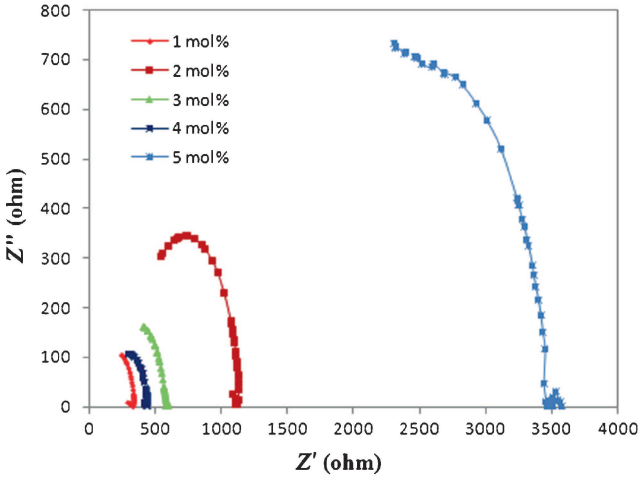

Figure 5. Cole–cole plot of $60V_2O_5$–$5P_2O_5$–$(35-x)B_2O_3$–$xCeO_2$ at 393 K.

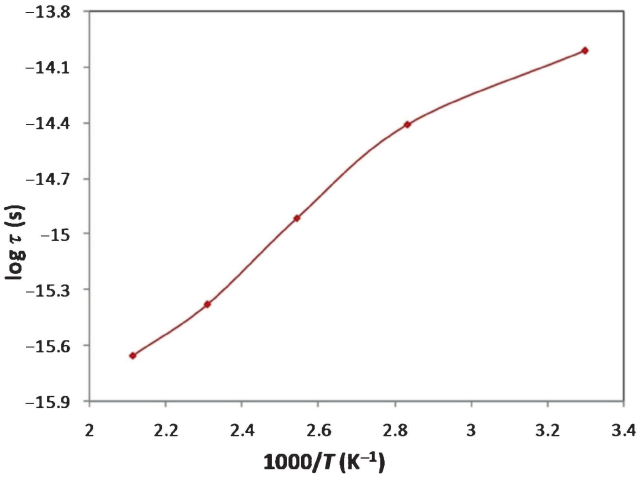

Figure 6. Plot between relaxation time and inverse of temperature for $60V_2O_5$–$5P_2O_5$–$33B_2O_3$–$2CeO_2$.

Table 1. DC conductivity (σ_{dc}), activation energy (E_{dc}), R, C and relaxation time (τ).

Sample	σ_{dc} at 303 K (S cm^{-1})	σ_{dc} at 473 K (S cm^{-1})	E_{dc} (eV)	R at 303 K (Ω)	C at 303 K (F)	τ at 303 K (s)
C1	0.0024	0.0089	0.09	390.4	4.08×10^{-10}	1.59×10^{-7}
C2	0.00032	0.0029	0.16	2376.7	3.44×10^{-10}	8.18×10^{-7}
C3	0.00067	0.0055	0.15	1111.8	2.72×10^{-10}	3.03×10^{-7}
C4	0.0012	0.0080	0.14	788.2	4.22×10^{-10}	3.32×10^{-7}
C5	3.26×10^{-5}	0.0007	0.22	9489.8	2.7×10^{-10}	2.56×10^{-7}

C1, C2, C3, C4 and C5 represent mol% of CeO_2 varying from 1 to 5 mol%.

This dispersion is largest at lower temperatures. It is seen from figure, as the temperature increases, the frequency at which dispersion becomes prominent, shifts to higher frequency region, which is analysed by using Jonscher's universal power law.[30,31]

$$\sigma(\omega) = \sigma(0) + A\omega^n, \tag{4}$$

where $\sigma(0)$ is the frequency-independent DC conductivity of the sample, A a weakly temperature-dependent quantity and n the power law exponent lying in the range $0 < n < 1$. The conductivity data of all glass compositions have been fitted to the above equation. Equation (4) shows good agreements with the experimental data.

Figure 9 shows the plots of Z'' as a function of frequency at different temperatures, which shows non-Debye-type peaks. This may be due to the existence of distributed relaxation times. With the increase in temperature, peak maxima (ω_m) are found to shift towards high frequency region. The above shift obeys the Arrhenius equation, which suggests ion transport follows the hoping mechanism.[20]

Figure 10 shows the frequency dependence plots of real part of dielectric constant ε' at various temperatures for glass composition $60V_2O_5$–$5P_2O_5$–$(35-x)B_2O_3$–$1CeO_2$. It is found that at a particular temperature the value of ε' decreases with the increase in frequency. This shows the contribution of charge carriers decreases with the increase in frequency and attains a constant value ε'_∞, which may be due to the effect of much more rapid polarization process in the sample. In low-frequency region, the value of ε' is high due to the presence of metallic or blocking electrodes, which accumulates charges at the electrode–sample interface. In the high frequency region, at low temperatures, the well-known non-Debye behaviour is observed. The observed

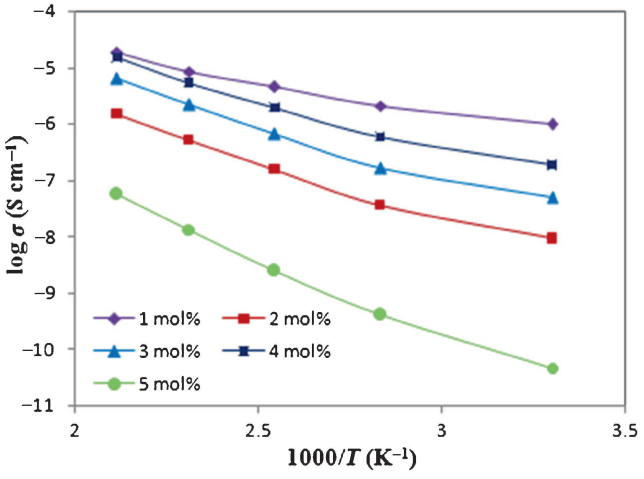

Figure 7. Temparatrure-dependent DC conductivity of $60V_2O_5$–$5P_2O_5$–$(35-x)B_2O_3$–$xCeO_2$.

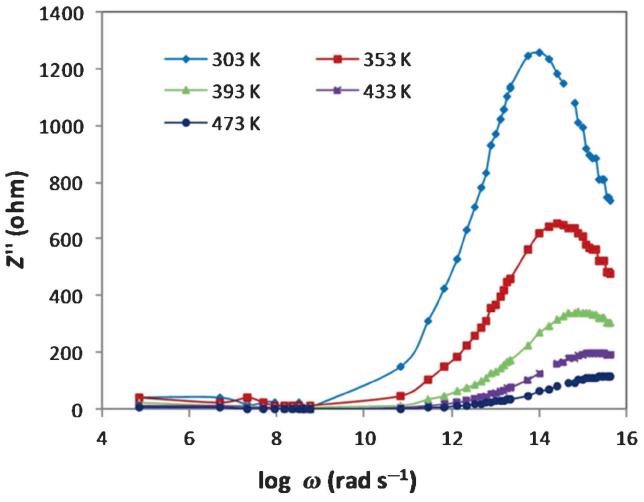

Figure 9. Plot of Z'' as a function of frequency for $60V_2O_5$–$5P_2O_5$–$(35-x)B_2O_3$–$1CeO_2$.

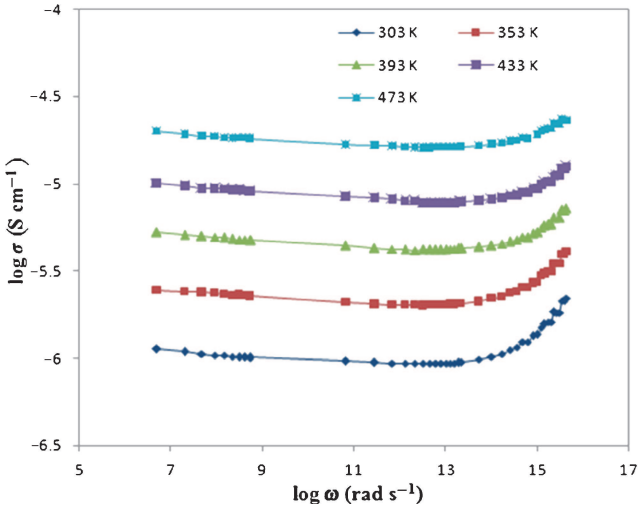

Figure 8. Frequency-dependent conductivity plot of $60V_2O_5$–$5P_2O_5$–$(35-x)B_2O_3$–$1CeO_2$.

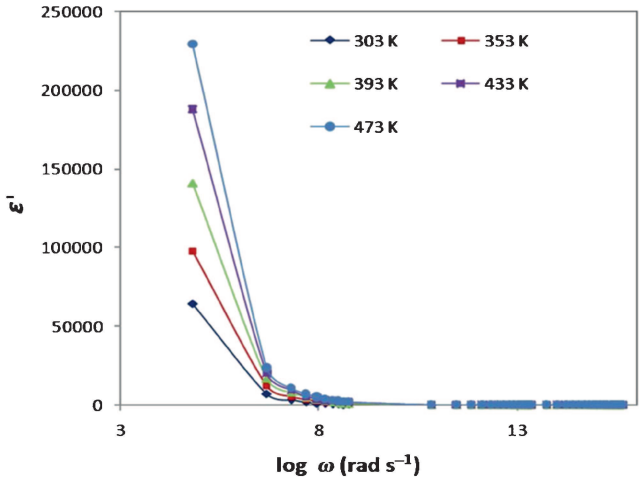

Figure 10. Frequency dependence plot of real part of dielectric constant for $60V_2O_5$–$5P_2O_5$–$(35-x)B_2O_3$–$1CeO_2$.

frequency dependence of ε' for other compositions shows similar nature.[23,32–35]

3.4 *Electric modulus*

The electric modulus is an approach to investigate the complex electrical responseof materials, which nullify the electrode polarization effect. Figure 11 shows the real part of modulus (M') *vs.* log(ω) for the composition $60V_2O_5$–$5P_2O_5$–$(35-x)B_2O_3$–$1CeO_2$ at different temperatures. At higher frequencies, M' reaches to maximum constant value and at low frequencies M' approaches to zero indicates that electrode polarization makes a negligible contribution. The dispersion in between these frequencies is due to the conductivity relaxation.

Figure 12 represents the imaginary part of electric modulus M'' *vs.* log(ω) spectra plotted at different temperatures for the composition $60V_2O_5$–$5P_2O_5$–$(35-x)B_2O_3$–$1CeO_2$. It is observed that the shape of each curve is non-Lorentzian type and with the increase in temperature, the peak frequency shifts towards the higher frequency region. It may be due to the distribution of attempt frequencies to penetrate the potential barrier.[1–4,34]

Figure 13 represents the Nyquist plot for the composition $60V_2O_5$–$5P_2O_5$–$(35-x)B_2O_3$–$1CeO_2$ at different temperatures, which shows the semi-arc with the center under M' axis. This may be due to the existence of a distribution of some physical characteristic of materials. This phenomenon is studied using a electronic circuit where a constant phase element is used. The impedance of this element is given by Equation (5)[36]

$$\frac{1}{Z_{CPE}} = Y_0(j\omega)^{\beta}, \tag{5}$$

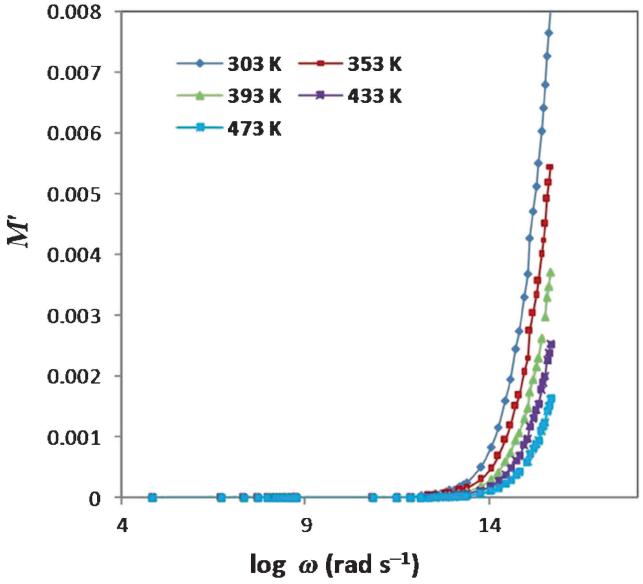

Figure 11. Real part of the modulus *vs.* log(ω) for the composition $60V_2O_5$–$5P_2O_5$–$(35-x)B_2O_3$–$1CeO_2$.

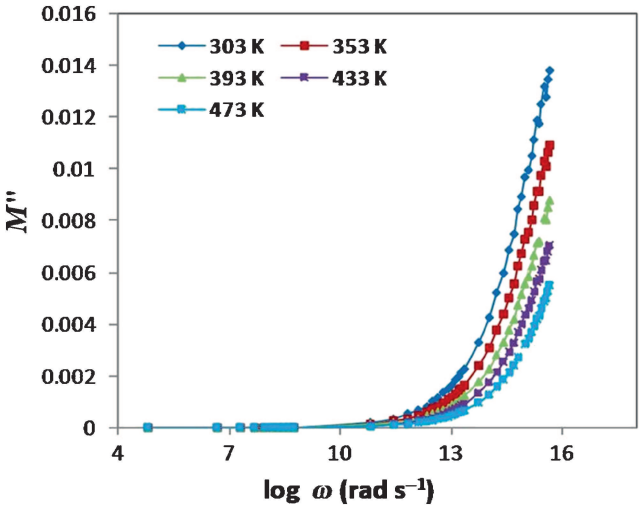

Figure 12. Imaginary part of the modulus *vs.* log(ω) for the composition $60V_2O_5$–$5P_2O_5$–$(35-x)B_2O_3$–$1CeO_2$.

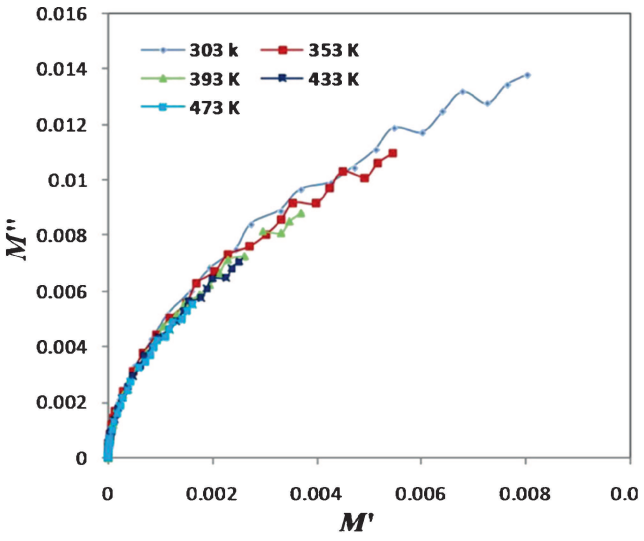

Figure 13. Nyquist plot of electrical modulus for $60V_2O_5$–$5P_2O_5$–$(35-x)B_2O_3$–$1CeO_2$.

where Y_0 is the admittance ($1/|Z|$) at $\omega = 1$ rad s^{-1} and β is a value between 0 and 1.

4. Conclusions

The melt-quenching technique is a very simple method for the preparation of conducting glasses. The amorphous nature of glasses was reflected from XRD study. The glass transition temperature (T_g) was observed to increase with CeO_2 content. The thermal stability was found to be excellent for the composition 1 mol% of CeO_2. The AC conductivity obeys a power law. The glass samples exhibit typical inorganic semiconducting behaviour. The activation energy and conductivity at room temperature were found to be 0.09 eV

and 0.0024 S cm^{-1}, respectively, for 1 mol% of CeO_2. The dielectric constant of the sample decreases with increasing frequency and increases with increasing temperature. The electrical modulus study reveals that the electrode polarization has negligible contribution.

Acknowledgement

We are thankful to Head, Department of Physics, Sant Gadge Baba Amravati University, Amravati and Principal H.V.P.M's College of Engineering and Technology for providing necessary facilities.

References

1. Barde R V and Waghuley S A 2013 *AIP Conf. Proc.* **1536** 609
2. Barde R V and Waghuley S A 2013 *Ceram. Int.* **39** 6303
3. Barde R V and Waghuley S A 2013 *Int. J. Mod. Phys.: Conf. Ser.* **22** 255
4. Barde R V and Waghuley S A 2013 *J. Non-Cryst. Solids* **376** 117
5. Subhadra M and Kistaiah P J 2011 *Phys. Chem. A* **115** 1009
6. Ramesh Babu A, Rajyasree Ch, Srinivasa Rao P, Vinaya Teja P M and Krishna Rao D 2011 *J. Mol. Struct.* **1005** 83
7. Pisarski W A, Goryczka T, Wodecka-Dus B, Plonska M and Pisarska J 2005 *Mater. Sci. Eng. B* **122** 94
8. Qiu J, Igarashi H and Makishima A 2005 *Sci. Technol. Adv. Mater.* **6** 431
9. Ansari A A, Kaushik A, Solanki P R and Malhotra B D 2008 *Electrochem. Commun.* **10** 1246
10. Guo H and Qiao Y 2008 *Appl. Surf. Sci.* **254** 1961
11. Murata T, Sato M, Yoshida H and Morinaga K 2005 *J. Non-Cryst. Solids* **351** 312
12. Laroche M, Girard S, Moncorge R, Bettinelli M, Abdulsabirov R and Semashko V 2003 *Opt. Mater.* **22** 147
13. PalSingh G and Singh D P 2011 *Physica B* **406** 3402
14. Moses W W, Derenzo S E, Fyodorov A, Korzhik M, Gektin A, Minkov B and Aslanov V 1995 *IEEE Trans. Nucl. Sci.* **42** 275
15. Mansour E 2011 *J. Non-Cryst. Solids* **357** 1364
16. Agrawal R C, Verma M L, Gupta R K and Kumar R 2002 *J. Phys. D: Appl. Phys.* **35** 810
17. Agrawala R C, Vermab M L and Gupta R K 2004 *Solid State Ionics* **171** 199
18. Waghuley S A 2011 *Indian J. Pure Appl. Phys.* **49** 816
19. Viswanathan A, Suthanthiraraj S A and Chowdari B V R 1992 *Solid State Ionics: Mater. Appl.* **379** 3
20. Bhide A and Hariharan K 2007 *Mater. Chem. Phys.* **5** 213
21. Zhang Q, Wen Z, Liu Y, Song S and Wu X 2009 *J. Alloys Compd.* **479** 494
22. El-Muraikhi M 2009 *Mater. Chem. Phys.* **116** 52
23. Vinoth Rathan S and Govindaraj G 2010 *Solid State Sci.* **12** 730
24. Deshpande S K, Shrikhande V K, Jogad M S, Goyal P S and Kothiyal G P 2007 *Bull. Mater. Sci.* **30** 497
25. Padmasree K P and Kanchan D K 2006 *J. Non-Cryst. Solids* **352** 3841
26. Deshpande V K, Pradel A and Ribbs M 1988 *Mater. Res. Bull.* **23** 379
27. Gedam R S and Deshpande V K 2006 *Solid State Ionics* **177** 2589
28. Alexander M N, Onorato P I K, Struck C W, Rozen J R, Tasker G W and Uhlmann D R 1986 *J. Non-Cryst. Solids* **79** 137
29. El-Desoky M M, Ibrahim F A, Mostafa A G and Hassaan M Y 2010 *Mater. Res. Bull.* **45** 1126
30. Jonscher A K 1977 *Nature* **267** 673
31. Mariappan C R, Govindaraj G, Vinoth Rathan S and Vijaya Prakash G 2005 *Mater. Sci. Eng. B* **121** 2
32. Jonscher A K 1983 *Dielectric relaxation in solids* (London: Chelsea Dielectric Press)
33. Macdonald J R 1987 *Impedance spectroscopy* (New York: Wiley)
34. Dutta A, Sinha T P, Jena P and Adak S 2008 *J. Non-Cryst. Solids* **354** 3952
35. Jayaseelan S, Muralidharan P, Venkateswarlu M and Satyanarayana N 2004 *Mater. Chem. Phys.* **87** 370
36. Grac M P F, Valent M A and Ferreira da Silva M G 2003 *J. Non-Cryst. Solids* **325** 267